Tuning the magneto-elastic transition of $(Mn,Fe,V)_2(P,Si)$ alloys to low magnetic field applications

Lai, Jiawei; You, Xinmin; Dugulan, Iulian; Huang, Bowei; Liu, Jun; Maschek, Michael; van Eijck, Lambert; van Dijk, Niels; Brück, Ekkes

DOI
10.1016/j.jallcom.2019.153451

Publication date
2020

Document Version
Final published version

Published in
Journal of Alloys and Compounds

Citation (APA)
Lai, J., You, X., Dugulan, I., Huang, B., Liu, J., Maschek, M., van Eijck, L., van Dijk, N., & Brück, E. (2020). Tuning the magneto-elastic transition of $(Mn,Fe,V)_2(P,Si)$ alloys to low magnetic field applications. *Journal of Alloys and Compounds*, *821*, Article 153451. https://doi.org/10.1016/j.jallcom.2019.153451

Journal of Alloys and Compounds 821 (2020) 153451

Contents lists available at ScienceDirect

Journal of Alloys and Compounds

journal homepage: http://www.elsevier.com/locate/jalcom

Tuning the magneto-elastic transition of $(Mn,Fe,V)_2(P,Si)$ alloys to low magnetic field applications

Jiawei Lai*, Xinmin You, Iulian Dugulan, Bowei Huang, Jun Liu, Michael Maschek, Lambert van Eijck, Niels van Dijk, Ekkes Brück

Fundamental Aspects of Materials and Energy, Department of Radiation Science and Technology, TU Delft, Mekelweg 15, 2629JB, Delft, the Netherlands

ARTICLE INFO

Article history:
Received 9 July 2019
Received in revised form
3 December 2019
Accepted 18 December 2019
Available online 19 December 2019

Keywords:
Transition metal alloys and compounds
Phase transitions
Mössbauer spectroscopy
Neutron diffraction
Magnetocaloric

ABSTRACT

The first-order magneto-elastic transition in the Mn–Fe–P–Si alloys can be tailored by vanadium substitution. Alloys with a suitable V substitution provide an excellent magnetocaloric effect with minor hysteresis in low magnetic fields up to 1.2 T. Mössbauer measurements show that the hyperfine field is reduced by V substitution. Neutron diffraction reveals that Fe is substituted by V on the *3f* site and the magnetic moment on the *3f* site is enhanced by the V substitution. The modified magnetic exchange field around the *3f* and *3g* positions in the lattice can be utilized to design suitable magnetocaloric materials that operate in low magnetic fields.

1. Introduction

Based on the giant magnetocaloric effect (GMCE), novel technologies as magnetic heat pumps [1–3] and thermomagnetic motors [4,5] have been developed for caloric cooling and waste heat recovery. The GMCE is attributed to a first-order magneto-structural or magneto-elastic transition (FOMT), which has been found in e.g. $Gd_5(Ge,Si)_4$ [6], Heusler alloys [7], $La(Fe,Si)_{13}$ [8] and $(Mn,Fe)_2(P,Si)$ [9] alloys near room temperature.

Among these systems, the $La(Fe,Si)_{13}$ and $(Mn,Fe)_2(P,Si)$ alloys with an itinerant electronic meta-magnetic (magneto-elastic) transition are regarded as the most promising candidates for large-scale applications due to their excellent GMCE, abundant availability of the starting materials and a limited volume change, which provides the potential for a low hysteresis [10,11]. Since a strong FOMT generally has the drawback of large hysteresis which deteriorates the efficiency, it is of particular interest to tune the magneto-elastic transition towards the critical condition for a cross-over to a second-order magnetic transition (SOMT) without latent heat [12]. As a result, the GMCE can be largely preserved, while the hysteresis is minimized.

$(Mn,Fe)_2(P,Si)$ alloys crystallize in the Fe_2P-type hexagonal structure (space group *P-62 m*) [13,14]. The FOMT originates from an electronic redistribution around the *3f* site, which is preferentially occupied by the Fe atoms [14,15]. This electronic instability is accompanied by a reduction in the magnetic moment at the *3f* site (M_{3f}). The *3g* site, which is preferentially occupied by Mn, does not show an instability in the electronic structure and magnetic moment. This effect has been termed 'mixed magnetism' as strong magnetism coexist with weak magnetism in a single alloy [16]. The magneto-elastic transition in $(Mn,Fe)_2(P,Si)$ alloys can be tuned by other *3d* metals like Co, Ni, Cu [17,18], or metalloids like As, Ge [19,20], B [21], C [22], N [23]. In addition, the annealing conditions [24,25] also strongly affect the magneto-elastic transition in the Fe_2P-type alloys. Vanadium (V) substitution in the $(Mn,Fe)_2(P,Si)$ alloys has been investigated in detail and reveals that the magneto-elastic transition can be tuned to the critical condition where an enhanced GMCE was obtained [26]. However, the influence of V substitution on the evolution of the magnetic exchange-field between the magnetic atoms has not been investigated yet. These exchange fields are a key ingredient to understand how the magneto-elastic transition can be induced in low magnetic fields.

Neutron diffraction and Mössbauer spectroscopy were used to reveal the evolution of the magnetic moments and the hyperfine field in Mn–Fe–P–Si–V alloys. We show that V substitution shifts the FOMT towards the border to the SOMT, which results in a

* Corresponding author.
E-mail addresses: scutjiaway@gmail.com (J. Lai), e.h.bruck@tudelft.nl (E. Brück).

https://doi.org/10.1016/j.jallcom.2019.153451

reduction in the hyperfine field of the alloy and an increase in the local M_{3f}. These investigations pave the way to a better design of MCE materials for magnetic heat pumps and thermomagnetic motors that can operate in low applied magnetic fields.

1.1. Methods

Polycrystalline alloys were prepared by powder metallurgy. The starting materials, in the form of Mn (99.7%), Fe (99.7%), red P (99%), Si (99.7%) and V (99.5%) powders, were mechanically ball milled in a PULVERRISETTE 5 planetary mill for 10 h in an Ar atmosphere with a constant rotation speed of 380 rpm, then pressed into small tablets (ø 13 mm, mass 3−5 g), and finally sealed in quartz ampoules under 200 mbar of Ar. These tablets were then annealed at 1343 and 1373 K for 25 h and quenched into water. The samples are listed as follows: (*V0H*) $Mn_{1.17}Fe_{0.73}P_{0.5}Si_{0.5}$ alloys annealed at 1373 K, (*V2H*) $Mn_{1.17}Fe_{0.71}P_{0.5}Si_{0.5}V_{0.02}$ alloys annealed at 1373 K and (*V2L*) $Mn_{1.17}Fe_{0.71}P_{0.5}Si_{0.5}V_{0.02}$ alloys annealed at 1343 K.

X-ray diffraction (XRD) patterns were collected on a PANalytical X-pert Pro diffractometer with Cu-K_α radiation (1.54056 Å) at room temperature. The neutron diffraction data at 370 and 110 K were collected at a wavelength of 1.67105 Å on the neutron powder diffraction instrument PEARL [27] at the research reactor of Delft University of Technology. The temperature dependence of the magnetization was measured by a superconducting quantum interference device (SQUID) magnetometer (Quantum Design MPMS 5XL) in the reciprocating sample option (RSO) mode. The in-field DSC is measured in a Peltier cell based DSC using a Hallbach cylinder magnetic field ($\leq$1.5 T) with a scanning rate of 3.0 K/min. Transmission ^{57}Fe Mössbauer spectra were collected at 350 K with a conventional constant-acceleration spectrometer and at 110 K with a sinusoidal velocity spectrometer, using a ^{57}Co(Rh) source. A velocity calibration was carried out using α-Fe foil at room temperature. The source and the absorbing samples were kept at the same temperature during all measurements. The Mössbauer spectra were fitted using the Mosswinn 4.0 program [28]. All spectra were fitted with a binomial distribution model, as previously described for the Mössbauer spectroscopy experiments on $FeMnP_{1-x}As_x$ compounds [29].

2. Results

2.1. Magnetic properties

Fig. 1 shows the temperature dependence of the magnetization for samples *V0H*, *V2H* and *V2L* in a magnetic field of 1 T. The heating and cooling curves depict the thermal hysteresis (ΔT_{hys}), which is 1.5, 0.7 and 0.5 K for samples *V0H*, *V2H* and *V2L*, respectively. The Curie temperature (T_C), determined by the peak value of $-dM/dT$ in the heating curves, is 311.2, 290.1 and 289.7 K for samples *V0H*, *V2H* and *V2L*, respectively. An increase in the value of $-dM/dT$ for sample *V2H* measured at 1.0 T, shown in the inset of figure (a), indicates a higher magnetic entropy change ($-\Delta S_M$) at a low magnetic field change of 1.0 T. This is consistent with the $-\Delta S_M$ results at different magnetic field changes shown in Fig. 1(b). The $-\Delta S_M$ curves are extracted from heat capacity measurements in magnetic fields of 0, 0.5, 1.0 and 1.5 T. Open circle is the $-\Delta S_M$ extracted from magnetic measurement for sample *V2H* by applying the Maxwell equation to the iso-field magnetization under different magnetic field [26]. The $-\Delta S_M$ values obtained from the caloric and the magnetic measurement show good consistency. Particularly, sample *V2H* shows a larger value of $-\Delta S_M$ than sample *V0H* for the low magnetic field range up to 1.2 T. The value of $-\Delta S_M$ under a magnetic field of 1.0 T is 8.7, 9.2 and 6.8 J/kgK for *V0H*, *V2H*, and *V2L*, respectively. However, when the applied magnetic field increases to a higher magnetic field of 1.5 T, the value of $-\Delta S_M$ for *V2H* becomes lower than that of *V0H*, which is 11.7 and 12.7 J/kgK, respectively. This unusual field response will be addressed in the discussion section. The saturation magnetization measured at a temperature of 5 K for magnetic fields up to 5 T, shown in Fig. 1 (c), is 163.8, 156.7, 145.5 Am/kg for samples *V0H*, *V2H* and *V2L*, respectively.

3. Hyperfine interactions

The Mössbauer spectra measured at 350 and 110 K for the three samples are shown in Fig. 2. In the paramagnetic (PM) high-temperature phase, a single broad absorption line is observed. In the ferromagnetic (FM) low-temperature phase, a more complex absorption profile is observed that includes six rather broad spectral lines, which indicates a distribution in hyperfine field. Since P and Si are randomly distributed over the *2c* and the *1b* crystallographic positions, this leads to five inequivalent Fe nearest neighbors. In such a case the experimental Mössbauer spectra are usually fitted with a model that weighs the contribution of each Fe environment using a binomial distribution [29]. A similar model is used in this work and a summary of the derived average hyperfine parameters, together with the linewidth, and the fraction of the magnetic phase are given in Table 1.

At 110 K, most of the Fe species are ferromagnetic, with about 6% of the Fe atoms being still in the paramagnetic state. Interestingly, the hyperfine magnetic field is decreasing for V substitution from 22.3 T for sample V0L without vanadium to 21.9 and 21.7 T for vanadium containing samples *V2H* and *V2L*, respectively. The hyperfine magnetic field is only slightly decreasing for sample *V2L* compared to *V2H*, indicating that it is sensitive to the annealing temperature. The current Mössbauer data demonstrate that V is substituted into the Fe lattice and lowers the measured hyperfine field. The degree of substitution depends on the annealing temperature: the one annealed at 1343 K (*V2L*) has a higher degree than the one annealed at 1373K (*V2H*). According to the nominal sample composition, the V substitution is expected to result in a 2.7% reduction (= 0.02/0.73) in the Fe occupancy of the 3*f* site. When such a reduction is applied to the hyperfine field of Fe a value of 21.7 T is estimated for the vanadium containing samples.

4. X-ray diffraction and neutron diffraction

Rietveld refinement of XRD data for V2H sample at 370 K is shown in the Fig. 3 (a). The main phase is hexagonal Fe_2P-type phase (space group P-62 m) and the $(Mn,Fe)_3Si$-type phase (space group Fm3m) is identified as impurity phase. The volume fraction of impurity phase for samples *V0H*, *V2H* and *V2L* is 2.37 ± 0.51, 3.22 ± 0.58, 3.42 ± 0.95 vol%, respectively. Neutron diffraction measurements were performed for the *V0H*, *V2H* and *V2L* samples at temperatures of 370 and 110 K. The refinement pattern of *V2H* is illustrated in Fig. 3 (b) and the results are shown in Table 3. All samples are in the paramagnetic state at 370 K and in the ferromagnetic state at 110 K.

According to the Mössbauer results, there is still 6% of paramagnetic phase present at 110 K, which is different to the extracted fraction of impurity phase ($\approx$3%) from the XRD refinement results. This deviation is also observed in a previous Mössbauer study for the Mn−Fe−P−Si systems [14], which may be caused by a small fraction of amorphous phase, that is invisible to diffraction. The neutron diffraction patterns can be fitted with the Fe_2P-type hexagonal structure (space group *P-62 m*) with 4 different crystallographic sites, i.e. the *3f* and *3g* site for the Mn and Fe atoms and the *2c* and *1b* for the P and Si atoms, respectively [30]. The alignment of magnetic moment is within the *a-b* plane. The quality of Rietveld refinement in the paramagnetic state, indicates that V has a slight

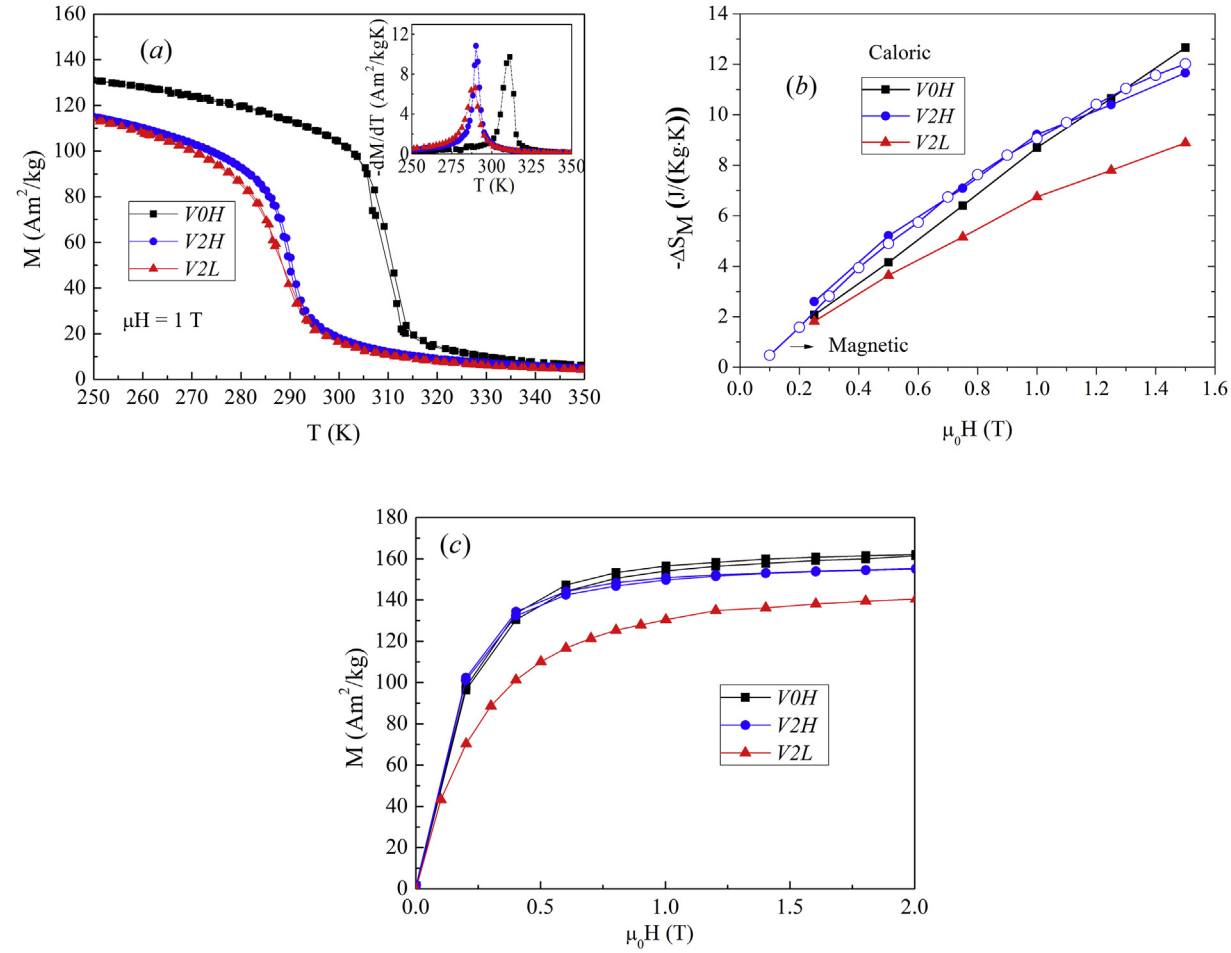

Fig. 1. (a) Magnetization as a function of the temperature measured in an applied magnetic field of 1 T with the $-dM/dT$ values shown in the inset; (b) magnetic entropy change $-\Delta S_M$ as a function of temperature for a magnetic field change up to 1.5 T (solid symbols are extracted from caloric measurement and open circles are extracted from magnetic measurement for sample *V2H*) and (c) Magnetization as a function of the applied magnetic field at a temperature of 5 K for samples *V0H*, *V2H* and *V2L*.

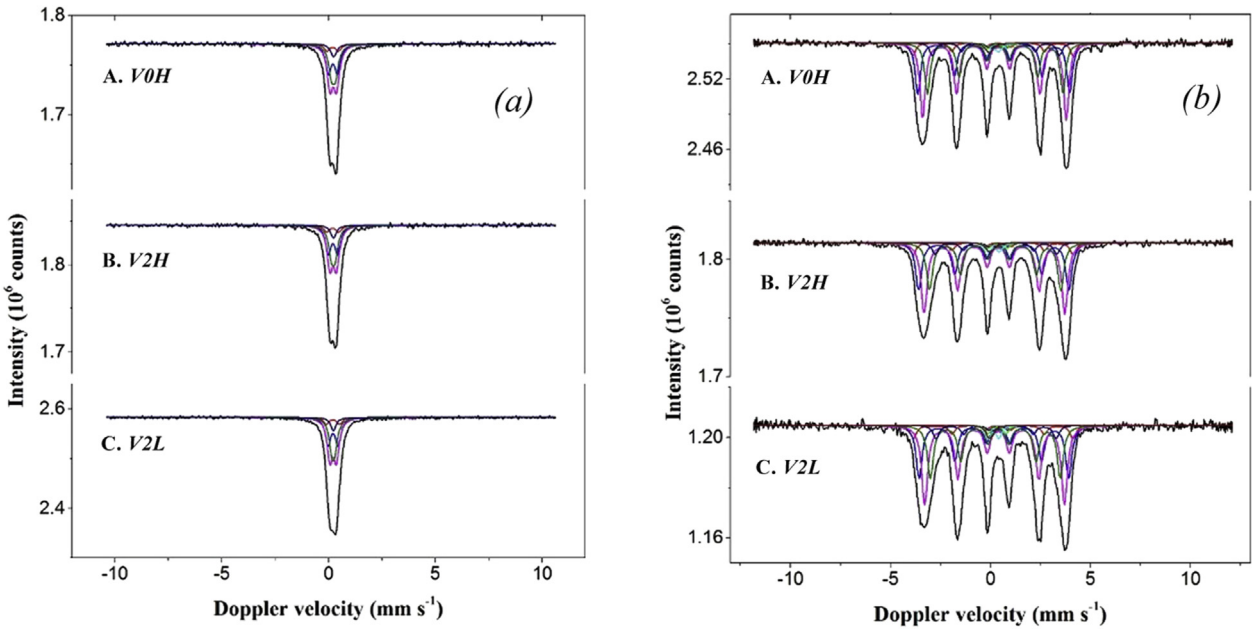

Fig. 2. Mössbauer spectra obtained for the magnetocaloric samples *V0H*, *V2H* and *V2L* at(a) 350 K and (b) 110 K.

Table 1
Mössbauer fit parameters for the magnetocaloric samples *V0H*, *V2H* and *V2L* at temperatures of 350 and 110 K.

Sample	T (K)	IS ($mm \cdot s^{-1}$)	QS ($mm \cdot s^{-1}$)	Hyperfine field* (T)	Γ ($mm \cdot s^{-1}$)	Phase	Spectral contribution (%)
V0H	350	0.22	0.31	–	0.32	P	100
V0H	110	0.29	−0.19	22.3	0.32	F	94
		0.14	0.53	–	0.42	P	6
V2H	350	0.21	0.31	–	0.32	P	100
V2H	110	0.29	−0.19	21.9	0.36	F	94
		0.15	0.56	–	0.41	P	6
V2L	350	0.21	0.31	–	0.30	P	100
V2L	110	0.29	−0.18	21.7	0.36	F	94
		0.15	0.54	–	0.40	P	6

Experimental uncertainties: Isomer shift: IS ± 0.01 mm s^{-1}; Quadrupole splitting: QS ± 0.01 mm s^{-1}; Line width: Γ ± 0.01 mm s^{-1}; Hyperfine field: ± 0.1 T; Spectral contribution: ± 3%; F/P: ferromagnetic/paramagnetic phases.

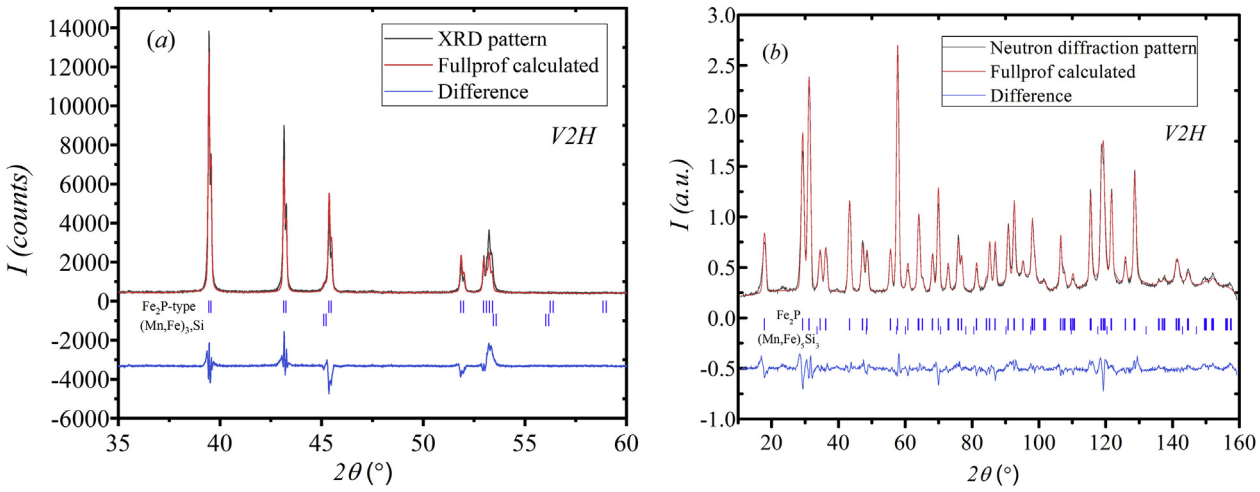

Fig. 3. XRD pattern at 370 K and Neutron diffraction at 110 K for the *V2H* sample.

preference to occupy the *3f* site rather than a random distribution on the Fe_2P-type lattice reported in a previous investigation [26]. For the ferromagnetic state in the current case of *V2H*, refinements have been conducted assuming that V is (i) all located exclusively on the *3f* site, (ii) located exclusively on the *3g* site or (iii) randomly distributed over the *3f* and *3g* sites and resulting in χ^2 values of 5.89, 6.89 and 6.51, respectively. Thus, the refinement results suggest that a better value of χ^2 is obtained when V is located on the *3f* site. And the calculated total magnetic moment is 3.9 ± 0.17, 3.5 ± 0.06 and 3.4 ± 0.06 μ_B, respectively. For the *V2L* sample, the value of χ^2 is 7.89, 7.64 and 6.39, respectively. And the calculated total magnetic moment is 3.9 ± 0.17, 3.9 ± 0.14 and 4.2 ± 0.15 μ_B, respectively. Note that the experimental spontaneous magnetic moment is 3.70 and 3.65 μ_B for the *V2H* and *V2L*, respectively. These results are summarized in Table 2. Obviously, here the value of χ^2 does not show significant variation on the different site occupancies. However, when considering the resulting magnetic moments of M_{3f} and M_{3g}, the calculated magnetic moments derived in the case of V on the *3f* shows a better agreement. Because a 63% reduction of M_{3f} would be an overestimation when V is located on either the *3g* or *3f* and *3g* randomly distribution. Thus, it is concluded that V has a preference to occupy the *3f* site.

The total refined magnetic moments are 4.2 ± 0.1, 3.9 ± 0.2 and 3.9 ± 0.2 μ_B for the *V0H*, *V2H* and *V2L* samples, respectively. These values are in agreement with the spontaneous magnetic moment (M_{total}) [31], calculated from the magnetization in the Fig. 1 (c), which decreases with the V content. The refined M_{3g} decreases from 2.6 μ_B for the *V0H* sample without V to 2.2 and 2.0 μ_B for the V containing samples *V2H* and *V2L*, respectively. The M_{3f} increases from 1.6 μ_B for the *V0L* sample without V to 1.7 and 1.9 μ_B for the V containing samples *V2H* and *V2L*, respectively. For the *V0H* alloys, which does not contain V, the neutron diffraction results are comparable to the previous published calculation for the Mn−Fe−P−Si system [30,32,33]. It suggests that our current refinement of neutron

Table 2
Neutron diffraction refined results of magnetic moment and χ^2 for assuming that V is (i) all located exclusively on the *3f* site, (ii) located exclusively on the *3g* site or (iii) randomly distributed over the *3f* and *3g* sites.

Sample	V position	M_{3f} (μ_B)	Er_{3f} (μ_B)	M_{3g} (μ_B)	Er_{3g} (μ_B)	M_{cal} (μ_B)	Er_{cal} (μ_B)	M_{total} (μ_B)	χ^2
V2H	*3f*	1.7	0.125	2.2	0.115	3.9	0.17	3.70	5.89
	3f+*3g*	0.9	0.046	2.6	0.032	3.5	0.04		6.51
	3g	0.9	0.047	2.6	0.032	3.5	0.04		6.59
V2L	*3f*	1.9	0.059	2.0	0.066	3.9	0.15	3.65	7.89
	3f+*3g*	2.3	0.104	1.6	0.090	3.9	0.14		6.39
	3g	1.8	0.131	2.4	0.120	4.3	0.17		7.64

Table 3
Refinement results from neutron diffraction at $T = 110$ K for the $Mn_{1.17}Fe_{0.73-x}P_{0.5}Si_{0.5}V_x$ alloys annealed at 1373 and 1343 K. Space group: *P*-62 *m*. Atomic positions: 3*f* (x_1,0,0), 3*g* (x_2,0,1/2), 2*c* (1/3,2/3,0), and 1*b* (0,0,1/2). The magnetic Moments are oriented within the *a*-*b* plane. The $M_{total}(\mu_B)$ values are extracted from the magnetization curves in Fig. 1 (c).

Site	Parameters	*V0H*	*V2H*	*V2L*
	a	6.210(6)	6.211(6)	6.203(6)
	c	3.296(6)	3.303(6)	3.303(6)
	V(Å)	110.09(3)	110.24(9)	110.09(4)
3*f*	x_1	0.25764(4)	0.25631(3)	0.25899(5)
	n(Fe)/*n*(Mn)/(V)	0.182/0.068/0.000(4)	0.190/0.055/0.050(6)	0.182/0.063/0.050(3)
	$\boldsymbol{M_{3f}(\mu_B)}$	**1.6 ± 0.094**	**1.7 ± 0.125**	**1.9 ± 0.059**
3*g*	x_2	0.59903(7)	0.59534(6)	0.59477(7)
	n(Mn)/*n*(Fe)	0.25/0.00	0.25/0.00	0.25/0.00
	$\boldsymbol{M_{3g}(\mu_B)}$	**2.6 ± 0.077**	**2.2 ± 0.115**	**2.0 ± 0.066**
	$\boldsymbol{M_{total}(\mu_B)}$	**4.2 ± 0.12**	**3.9 ± 0.17**	**3.9 ± 0.15**
2*c*	*n*(P)/*n*(Si)	0.092/0.074(4)	0.099/0.068(4)	0.091/0.076(0)
1*b*	*n*(P)/*n*(Si)	0.033/0.050(4)	0.026/0.057(1)	0.034/0.049(1)
	Rp(%)	5.39	5.02	5.62
	wRp(%)	6.95	6.49	7.48
	χ^2	9.30	5.82	7.89
	$\boldsymbol{M_s(\mu_B)}$	**4.01**	**3.70**	**3.65**

results are acceptable. Note that the magnetic moment of Mn—Fe—P—Si system containing V has not been reported yet. The higher moment on *3f* for *V2L* compared to the V free alloy, should be related to the introduction of V on *3f* site, that probably reduces the hybridization of *3d* states with Si *p* states. The *V2L* sample shows a negligible thermal hysteresis of 0.5 K, which suggest that it is very close to the SOMT. This is different from the previous reported samples with FOMT. The previous neutron data also showed an increase of M_{3f} when the first order phase transition is weakened [30].

5. Discussion

The latent heat is generally regarded as a sign of the strength of FOMT [10]. The latent heat, extracted from the heat capacity curves in Fig. 4 (a), is 9.3, 6.3, 5.6 kJ/kg for samples *V0H*, *V2H* and *V2L*, respectively. These values indicate that the strength of the first-order magneto-elastic transition is weakened by the V substitution. The phenomenon that −dM/dT of *V2H* is sharper and larger than that of *V0H* is observed at 1.0 T, which suggest a better performance for the *V2H* under 1.0 T. This result is consistent with the entropy change shown in the Fig. 1 (b). When comparing the $-\Delta S_M$ under a higher magnetic field of 1.5 T, the $-\Delta S_M$ value of *V2H* is lower than *V0H*. On the other hand, the latent heat of *V2H* is smaller than *V0H*. This is because the latent heat indicates the lattice contribution to $-\Delta S_M$. However, $-\Delta S_M$ includes both lattice and spin (magnetic and electronic) contribution [34]. The larger -dM/dT or entropy change of *V2H* suggests a lager magnetic contributions is induced at a low field range than the one in *V0H*. As shown the Fig. 1(*c*), the magnetic permeability of *V2H* is also enhanced by V substitution. In comparison to sample *V0H* without V, the magnetization saturates in a lower field for sample *V2H* with V.

Since ΔT_{hys} correlates to both intrinsic and extrinsic properties [27] and the amount of impurity phase of the current samples is essentially at the same level, the value of ΔT_{hys} here represents the strength of the magneto-elastic coupling, i.e. how strong the FOMT is. Therefore, it is interesting to investigate the magnetic moments and the hyperfine fields as functions of ΔT_{hys}. Fig. 4 (b) shows the dependence of ΔT_{hys} with the hyperfine field (diamond) and M_{total} (triangle), M_{3g} (Rectangle) and M_{3f} (cycle) in the ferromagnetic state. The reduced hyperfine field is consistent with the weakened FOMT on substituting Fe by V as indicated by the latent heat results. However, the trend of hyperfine field differs somewhat from the trend of M_{total}, but is in good agreement with the trend of M_{3g}. This phenomenon can be explained by the mixed magnetism in the Fe_2P-type alloys. The meta-magnetic behavior of binary Fe_2P alloys have been investigated theoretically by Yamada et al. [35] According to Landau—Ginzburg theory, the ferromagnetic state of Fe atoms on the *3f* site is stabilized by the exchange field from the magnetic Fe atoms on the *3g* site. Therefore, the exchange field is governed by M_{3g}. In consequence, a small moment of 0.3 μ_B is

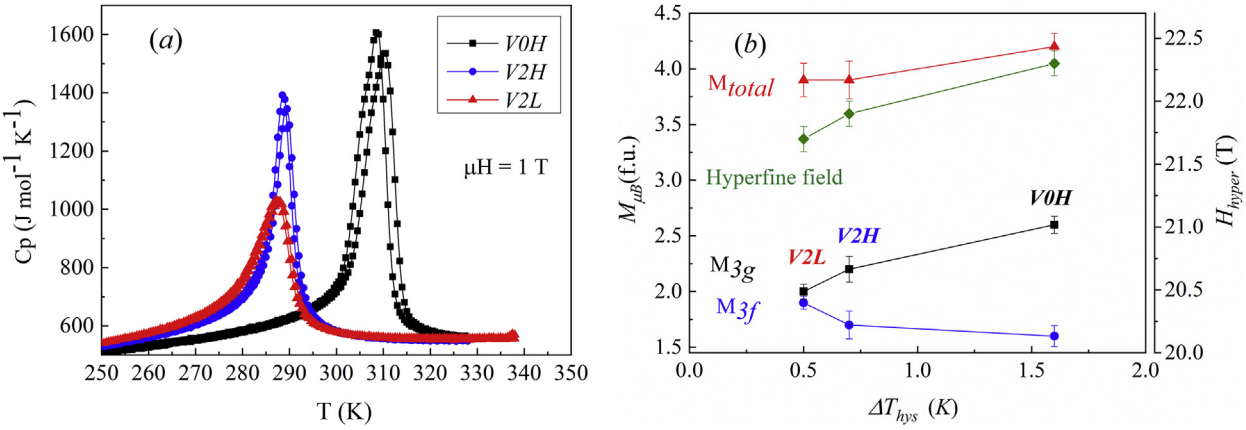

Fig. 4. (a) Heat capacity in a magnetic field of 1.0 T for the *V0H*, *V2H* and *V2L* samples. (b) Hyperfine field (diamond) and M_{total} (triangle), M_{3g} (Rectangle) and M_{3f} (cycle) in the ferromagnetic state.

induced on Fe(*3f*) and a moment of 0.4 μ_B is induced on Fe(*3g*) in the binary Fe_2P alloys. Therefore, in the current Mn—Fe—P—Si—V system, the trend of M_{3g} determines the trend of exchange field, as shown in Fig. 4 (*b*).

As mentioned above, in the binary Fe_2P alloy, M_{3f} is affiliated with the change of M_{3g}, i.e. a reduced M_{3g} will result in a weaker M_{3f} [35]. Astonishingly, M_{3f} in the current Mn—Fe—V—P—Si system is raised when M_{3g} is reduced, see Fig. 4 (b). It suggests a minor addition of V in the quaternary alloy complicates the magnetic coupling in the Fe_2P-type structure. The mechanism of the enhanced magnetic moment of M_{3f} can be explained through the competition between bond formation (*3d-2p* hybridization) and moment formation since this is the intrinsic basis of the FOMT in the Fe_2P type structure [15]. A strong FOMT will show a strong bond formation and a weak moment formation on the *3f* site. The decrease of the hyperfine field and latent heat suggests that bond formation is weakened by V substitution. As a result, the moment formation is strengthened. Thus, the preference of moment formation instead of bond formation on the *3f* site should be the intrinsic origin of high M_{3f}. In the current experimental method, we directly observed that the increase is caused by adding the V on the *3f* site. To better understand the mechanism of it, more experimental probes like x-ray magnetic circular dichroism (XMCD) [36], which can clarify the role of each Mn, Fe and V atoms on the *3f* site, and theoretical calculations are necessary to reveal the mechanism behind it. The enhancement of M_{3f} makes it possible to lower the magnetic field inducing the FOMT. As a result, sample *V2H* shows a larger value of $-\Delta S_M$ than the sample *V0H* for the low magnetic field range up to 1.2 T. The current mechanism suggests that enhancing M_{3f} can bring a better low-field MCE, which enables the design of suitable MCE materials that operate in low magnetic fields. Further decreasing the exchange field in sample *V2L* will approach the critical region. The character of FOMT for *V2L* becomes insufficient and a nearly second-order magnetic phase transition is found, as indicated by the heat capacity in Fig. 4 (a).

6. Conclusions

V substitution in the Mn—Fe—P—Si alloys makes it feasible to tune the magento-elastic transition towards the critical point between FOMT and SOMT. A decreasing hyperfine field proves that the magnetic exchange field between the magnetic *3f* and *3g* sites in the Fe_2P-type structure is decreased, which lowers the total magnetic moment. V is found to occupy the *3f* site and results in the development of an enhanced M_{3f}. The mechanism of the enhanced M_{3f} is the reduction of *3d-2p* hybridization or bonding on the *3f* site when introducing V. In consequence, the magnetic contribution of the entropy change is increased and an enhanced MCE below 1.2 T is achieved in the sample *V2H*.

Author contribution

Jiawei Lai, Writing - original draft;; Investigation; Methodology; Validation;

Xinmin You,; Investigation; Methodology; Validation;

Iulian Dugulan, Mössbauer Data curation; Formal analysis;

Bowei Huang,; Investigation; Methodology;

Jiu Liu,; Investigation; Methodology;

Michael Maschek,; Investigation; Methodology;

Lambert van Eijk, Neutron diffraction Resources; Software; Supervision; Validation;

Niels van Dijk, Conceptualization; Supervision; Writing - review & editing.

Ekkes Brück Funding acquisition, Conceptualization; Supervision; Writing - review & editing.

Acknowledgements

The authors acknowledge Anton Lefering, Kees Goubitz, and Bert Zwart for their technical assistance. This work has been financially supported by the Dutch national research organization NWO TTW.

References

[1] K.A. GschneidnerJr, V.K. Pecharsky, A.O. Tsokol, Rep. Prog. Phys. 68 (2005) 1479.
[2] E. Brück, O. Tegus, D.T.C. Thanh, K.H.J. Buschow, J. Magn. Magn. Mater. 310 (2007) 2793.
[3] B.G. Shen, J.R. Sun, F.X. Hu, H.W. Zhang, Z.H. Cheng, Adv. Mater. 21 (2009) 4545.
[4] T. Christiaanse, E. Brück, Metall. Mater. Trans. A 1 (2014) 36.
[5] A. Waske, D. Dzekan, K. Sellschopp, D. Berger, A. Stork, K. Nielsch, S. Fähler, Nature Energy 4 (2018) 68.
[6] A.J.S. Virgil Provenzano, Robert D. Shull, Nature 429 (2004) 853.
[7] T. Krenke, E. Duman, M. Acet, E.F. Wassermann, X. Moya, L. Manosa, A. Planes, Nat. Mater. 4 (2005) 450.
[8] A. Fujita, Y. Akamatsu, K. Fukamichi, J. Appl. Phys. 85 (1999) 4756.
[9] X.-F. Miao, S.-Y. Hu, F. Xu, E. Brück, Rare Met. 37 (2018) 723.
[10] F. Guillou, G. Porcari, H. Yibole, N. van Dijk, E. Brück, Adv. Mater. 26 (2014) 2671.
[11] K. Navickaitė, H.N. Bez, T. Lei, A. Barcza, H. Vieyra, C.R.H. Bahl, K. Engelbrecht, Int. J. Refrig. 86 (2018) 322.
[12] O. Gutfleisch, et al., Philos. Trans.Ser. A .Math. Phys. Eng. Sci. 374 (2016).
[13] H. Yibole, F. Guillou, Y.K. Huang, G.R. Blake, A.J.E. Lefering, N.H. van Dijk, E. Brück, Appl. Phys. Lett. 107 (2015) 162403.
[14] D. Bessas, H. Yibole, J.W. Lai, S.M. Souliou, I. Sergueev, A.I. Dugulan, N.H. van Dijk, E. Brück, Phys. Rev. B 97 (2018), 094303.
[15] M.F.J. Boeije, F. Guillou, H. Yibole, F. Miao, L. Caron, D. Banerjee, N.H. van Dijk, R.A. de Groot, E. Brück, Chem. Mater. 28 (2016) 4901.
[16] N.H. Dung, Z.Q. Ou, L. Caron, L. Zhang, D.T.C. Thanh, G.A. de Wijs, R.A. de Groot, K.H.J. Buschow, E. Brück, Adv. Energy.Mater. 1 (2011) 1215.
[17] Z.Q. Ou, N.H. Dung, L. Zhang, L. Caron, E. Torun, N.H. van Dijk, O. Tegus, E. Brück, J. Alloy. Comp. 730 (2018) 392.
[18] N.V. Thang, N.H.V. Dijk, E. Brück, Materials 10 (2016) 14.
[19] H. Yibole, F. Guillou, L. Zhang, N.H. van Dijk, E. Brück, J. Phys. D Appl. Phys. 47 (2014), 075002.
[20] O. Tegus, E. Brück, K.H.J. Buschow, F.R. de Boer, Nature 415 (2002) 150.
[21] F. Guillou, H. Yibole, G. Porcari, L. Zhang, N.H. van Dijk, E. Brück, J. Appl. Phys. 116 (2014), 063903.
[22] N.V. Thang, H. Yibole, X.F. Miao, K. Goubitz, L. van Eijck, N.H. van Dijk, E. Brück, JOM 69 (2017) 1432.
[23] N.V. Thang, X.F. Miao, N.H. van Dijk, E. Brück, J. Alloy. Comp. 670 (2016) 123.
[24] N.V. Thang, H. Yibole, N.H. van Dijk, E. Brück, J. Alloy. Comp. 699 (2017) 633.
[25] J.W. Lai, et al., J. Alloy. Comp. 735 (2018) 2567.
[26] J. Lai, et al., J. Alloy. Comp. 803 (2019) 671.
[27] L. van Eijck, G.J. Sykora, E.M. Schooneveld, N.J. Rhodes, A.A.v. Well, C. Pappas, J. Appl. Crystallogr. 49 (2016) 1398.
[28] Z. Klencsár, Nucl. Instrum. Methods Phys. Res. B 129 (1997) 527.
[29] R.P. Hermann, E. Brück, K.H.J. Buschow, F.R. de Boer, G.J. Long, F. Grandjean, Phys. Rev. B 70 (2004) 214425.
[30] X.F. Miao, L. Caron, P. Roy, N.H. Dung, L. Zhang, W.A. Kockelmann, R.A. de Groot, N.H. van Dijk, E. Brück, Phys. Rev. B 89 (2014) 174429.
[31] J.W. Lai, Z.G. Zheng, R. Montemayor, X.C. Zhong, Z.W. Liu, D.C. Zeng, J. Magn. Magn. Mater. 372 (2014) 86.
[32] L. Zhang, O. Može, K. Prokeš, O. Tegus, E. Brück, J. Magn. Magn. Mater. 290–291 (2005) 679.
[33] N.H. Dung, et al., Phys. Rev. B 86 (2012), 045134.
[34] J. Lyubina, J. Phys. D Appl. Phys. 50 (2017), 053002.
[35] H. Yamada, K. Terao, Phase Transitions 75 (2002) 231.
[36] H. Yibole, F. Guillou, L. Caron, E. Jiménez, F.M.F. de Groot, P. Roy, R. de Groot, N.H. van Dijk, E. Brück, Phys. Rev. B 91 (2015), 014429.